GDCh Research Article Angewandte International Edition Chemie www.angewandte.org

How to cite: *Angew. Chem. Int. Ed.* **2024**, e202413122
doi.org/10.1002/anie.202413122

Microdroplet Chemistry Hot Paper

Programmable C–N Bond Formation through Radical-Mediated Chemistry in Plasma-Microdroplet Fusion

*Alexander J. Grooms, Robert T. Huttner, Mackenzie Stockwell, Leah Tadese, Isabella M. Marcelo, Anthony Kass, and Abraham K. Badu-Tawiah**

Abstract: Non-thermal plasma discharge produced in the wake of charged microdroplets is found to facilitate catalyst-free radical mediated hydrazine cross-coupling reactions without the use of external light source, heat, precious metal complex, or trapping agents. A plasma-microdroplet fusion platform is utilized for introduction of hydrazine reagent that undergoes homolytic cleavage forming radical intermediate species. The non-thermal plasma discharge that causes the cleavage originates from a chemically etched silica capillary. The coupling of the radical intermediates gives various products. Plasma-microdroplet fusion occurs online in a programmable reaction platform allowing direct process optimization and product validation via mass spectrometry. The platform is applied herein with a variety of hydrazine substrates, enabling i) self-coupling to form secondary amines with identical N-substitutions, ii) cross-coupling to afford secondary amine with different N-substituents, iii) cross-coupling followed by in situ dehydrogenation to give the corresponding aryl-aldimines with two unique N-substitutions, and iv) cascade heterocyclic carbazole derivatives formation. These unique reactions were made possible in the charged microdroplet environment through our ability to program conditions such as reagent concentration (i.e., flow rate), microdroplet reactivity (i.e., presence or absence of plasma), and reaction timescale (i.e., operational mode of the source). The selected program is implemented in a co-axial spray format, which is found to be advantageous over the conventional one-pot single emitter electrospray-based microdroplet reactions.

[*] Dr. A. J. Grooms, R. T. Huttner, M. Stockwell, L. Tadese, I. M. Marcelo, A. Kass, Prof. Dr. A. K. Badu-Tawiah
Department of Chemistry and Biochemistry
The Ohio State University
Columbus, OH 43210 (USA)
E-mail: badu-tawiah.1@osu.edu

Introduction

Radical chemistry offers many advantages over classical reactions based on ionic intermediates, including the ability to use neutral conditions, which avoid decomposition of pH-sensitive organic compounds.[1] However, the use of radical species in chemical synthesis often lacks selectivity. This long-standing synthetic challenge has motivated the development of innovative photochemical[2,3] (based on visible light) and electrochemical[4,5] tools to access radicals more mildly compared with traditional approaches that require radical initiation by azobisisobutyronitrile, alkyl tin, peroxides, or UV light. Fundamentally, only a few mechanisms for radical generation are available, utilizing one of three elementary steps: 1) hydrogen (H) abstraction via H atom transfer, 2) halide abstraction by homolytic bond cleavage, and 3) radical addition to an olefin bond.[6] For controlled and efficient intermolecular reactions, the generated radicals are often trapped; otherwise, self-coupling dominates irrespective of the means by which the radical was generated.[7] Without the use of trapping agents, we showcase in the current study that selective cross-coupling of free radicals can be achieved in charged microdroplet environment to afford a facile approach to rapidly control the formation of C–N bonds. The result of this approach is the programmable synthesis of secondary amines from homolytic cleavages of N–N and C–N bonds in hydrazines, without using catalysts or trapping agents. The energy required to break these bonds (including ~2.6 eV needed for cleaving the N–N bond)[8] is supplied by fusing nonthermal plasma (i.e., electrical discharge) with charged microdroplets.[9] We demonstrate that the desired product can be programmed by enabling cross-coupling, while excluding self-coupling, through the control of three interrelated factors: (1) microdroplet reactivity, as determined by the presence or absence of electrical discharge, (2) concentrations of reagents, as determined by relative flow rates in the electrospray process, and (3) timescale of microdroplet reactivity, as determined by the operational modes of our reconfigurable contained-electrospray source utilized for plasma-microdroplet fusion.

Important aspects of the current study take advantage of recent advancements in mass spectrometry (**MS**) in which electrospray ionization (**ESI**) now allows preparative scale chemical syntheses in the ensuing charged liquid microdroplets under ambient conditions rather than the use of gas-phase ions under high vacuum. In this case, charged microdroplets (with size measuring on the order of magnitude of 1–10 μm) bridge the gap between isolated gas-phase

ions and completely solvated species in bulk solution—thereby facilitating unique reaction enhancement in the confined-volume medium. In 2006, Eberlin and colleagues[10,11] showed the potential of electrosprayed microdroplets as a reaction platform in a transacetalization reaction. But, it was the Cooks group that first showcased the use of microdroplet chemistry for reaction acceleration in 2011.[12] Since this implementation, the field has expanded substantially—using the unique confined-volume medium for the investigation of addition (e.g. aza-Michael addition),[13] elimination (e.g., dehydration),[14] addition and elimination (e.g., Schiff base formation,[15] Katritzky transamination,[16] and Claisen–Schmidt condensation[17]), and oxidation (e.g., amine oxidation)[14] reactions to name a few. The mechanism behind charged microdroplet reactivity has also been the topic of many investigations that have showcased interfacial electric field enhancement,[18,19] high surface-area-to-volume ratio,[20] reactant confinement and concentration in small volumes,[21] and extreme pH effects as factors contributing to reaction enhancement.[22] In the past few years—there has been an influx of high impact investigations focusing specifically on the special properties of water microdroplets, alone. Investigators have proposed a higher degree of reaction enhancement from water microdroplets—attributed to enhanced interfacial electric field and production of reactive chemical species (e.g., hydroxyl radical)—which have facilitated numerous spontaneous chemical transformations not otherwise possible in bulk solution-phase.[22–36] Additional recent studies highlight the importance of the strong (10^8 V/cm) electric field on reaction acceleration and the formation of reactive species at the air-microdroplet interface.[37–40]

It has become clear that a great number of chemical transformations—known reactions and novel examples—are translatable in the charged microdroplet regime. Interestingly, most of these studies involve one-step chemical transformations giving rise to structurally homogeneous products without the ability to select unique moiety substitution within the final product. Use of the "one-pot" method for microdroplet synthesis whereby all reagent is sprayed through a single electrospray emitter has limited the ability to design chemical species with unique moiety functionalization due to the non-selectivity of one-pot spray yielding side products (i.e., self-coupled products) in addition to the desirable structurally heterogeneous products (i.e., cross-coupled products)—which are often the products of pharmacological importance.[41–43] Scheme 1A describes this one-pot conundrum, which we aim to overcome herein by introducing novel reaction selectivity for the production of select structurally heterogeneous C–N bond forming products via uncatalyzed hydrazine cross-coupling in the medium of charged microdroplets in a programmable, co-axial reaction platform (Scheme 1B).

Herein we utilize a programmable microdroplet-based co-axial reaction platform based upon uncatalyzed C–N bond formation. C–N bond formation is of ubiquitous importance across multiple fields of chemical science.[44–50] Efficient and widely applied methods for C–N bond formation include substituted reactions such as the

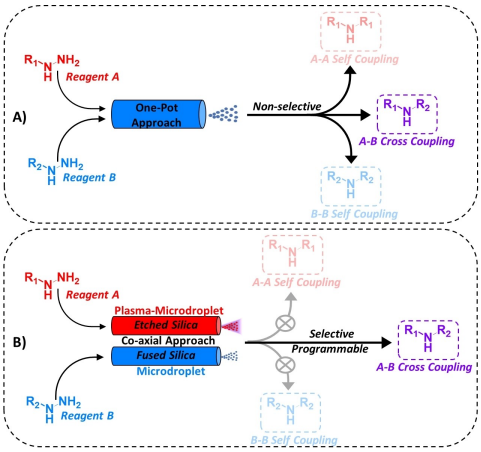

Scheme 1. Comparison of electrospray-based reaction platforms with **A**) one-pot approach (reagents pre-mixed before electrospray) giving a mixture of self-coupling structurally homogeneous products without selectivity, and **B**) co-axial spray approach giving selective programming for the cross-coupled heterogeneous product with minimal side reactions.

Ullmann,[51] Buchwald–Hartwig,[52] and hydroamination reactions,[53] along with metal-coordinated reactions.[54] Free radical reactions in nitrogenous systems have also represented a pathway for C–N bond formation.[55] As discussed above, conventional methods for free radical generation use radical initiators such as azobisisobutyronitrile catalysis, boiling organic solvent, and hydride reagent (e.g., tri-*n*-butyltin hydride)[56] making them unsustainable and thus driving the field toward greener synthetic pathways. Recent work towards this point has included the use of recyclable Pt catalysis for direct secondary amine synthesis[57] and metal-free, oxidant-free electrochemical C–N bond formation after extended (18 h) reaction.[58] We aim to continue the push towards green synthetic methods by using charged water microdroplets.

The confined environment of charged water microdroplets provide the medium for reaction via a tunable contained-electrospray (c-ESI) platform that is capable of fusing/mixing charged water microdroplets with energetic electrons and reactive oxygen species (ROS) derived from non-thermal plasma discharge in real time. The synergistic combination of water microdroplets with energetic electron collisions in plasma discharge to enhance internal energy deposition[9] occurs in a co-axial spray fashion (Scheme 1B) using two functionally unique capillaries: i) a chemically etched silica capillary for generation of plasma in the wake of charged microdroplets during ESI and ii) a deactivated fused silica capillary for generation of pure water microdroplet. On its own, non-thermal plasma discharge has recently gained interest in chemical synthesis and have been applied for reactions capable of utilizing the high energy species (e.g., electrons, excited state molecules, ions, and radicals) that exist within plasma.[9,59–61] Unfortunately, gas-phase plasma chemistry is limited in both scale-up and tunability/selectivity. The fusion of plasma discharge with charged microdroplet, as demonstrated here, has potential

to overcome these limitations by allowing opportunities for scale-up via condensed microdroplet collection and reaction tunablility, all on a single c-ESI platform. In this work, we focus on selectivity/programmability in plasma related reactions.

Programmable C–N bond formation is showcased herein concomitantly with cascade cyclization reactions for heterocyclic carbazole compound formation in a three-tier approach that builds upon fundamental C–N bond forming reactions via hydrazine coupling. The first set of experiments involved translating radical mediated hydrazine coupling from the gas-phase plasma discharge regime[59] to the condensed phase fusion of plasma in charged microdroplets. The collisions responsible for radical generation is achieved in situ via plasma discharge derived from a chemically etched silica capillary, which is capable of sustaining charged water microdroplet evolution. In this initial optimization study, the single hydrazine substrate undergoes homolytic dissociation yielding reactive radical intermediates—facilitated by enhanced internal energy deposition via the plasma-microdroplet source, exceeding the ~2.6 eV activation barrier to hydrazine N–N breakage.[9] Subsequent carbon-containing radical intermediates are observed to combine to give the corresponding secondary amine in a self-coupling process. The complexity of our study was then increased from self-coupling to cross-coupling reactions through the programmable C–N bond formation in which structurally unique hydrazine substrates were introduced into the plasma-microdroplet environment by changing concentration, droplet reactivity, and timescale of reaction via a co-axial spray platform. Through the programming of these three parameters, we achieved selective formation of C–N cross products across a wide range of structurally diverse substrates. Finally, we investigated microdroplet-phase Borsche–Drescel (B–D) cyclization. B–D cyclization is a type of cascade/multi-step reaction for carbazole formation that is achieved in bulk solution-phase by heating the reaction mixture (i.e., hydrazine and ketone) in the presence of concentrated acid.[62] Through the use of the programmable emitter, we achieved final product selectivity —avoiding unwanted side reactions (including hydrazine self-coupling) to facilitate select Schiff base formation followed by heterocycle B–D product formation, all in microdroplets. The main feature distinguishing our plasma-microdroplet reaction system from traditional method is related to the combined effects energetic collisions and unique chemical environment involving ROS, which can facilitate different reaction mechanisms simultaneously.

Results and Discussion

Platform for Programmable C–N Bond Formation

The plasma-microdroplet fusion platform utilized for the uncatalyzed C–N cross coupling reactions is as shown in Figure 1A. This co-axial c-ESI source was created in-house for simultaneous introduction of two solution-phase reagents via two functionally unique, co-axial capillaries. Hydrazine

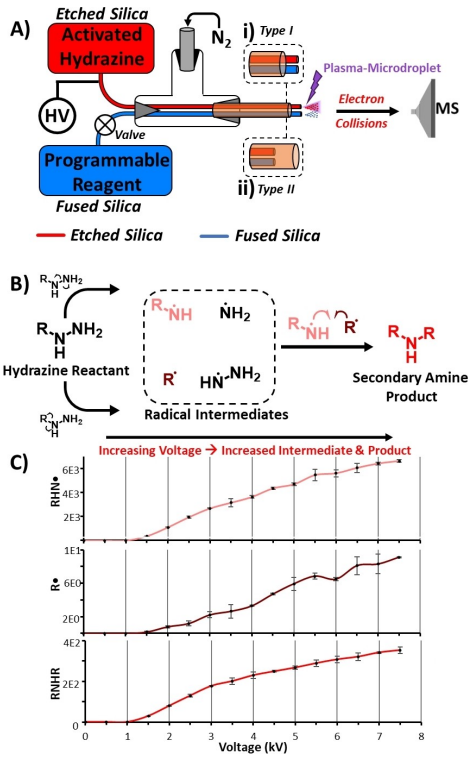

Figure 1. Platform for programmable plasma-microdroplet fusion for C–N bond formation with **A**) co-axial c-ESI setup with etched and fused silica spray capillaries for online plasma-microdroplet mixing, **B**) general reaction scheme for the radical mediated coupling of hydrazines for the formation of secondary amines, **C**) current/voltage mechanistic study evaluating the effect of spray voltage on intermediate and final product absolute abundance.

species were introduced through a chemically etched silica spray capillary (red line, Figure 1A**)**, produced in-house via hydrofluoric acid etching (details in **Supporting Information**). A programmable reagent (e.g., structurally diverse hydrazine) may be introduced via a deactivated fused silica capillary (blue line, Figure 1A) through the formation of charged water microdroplets. Importantly a valve is in place along the fused silica line to control the introduction of this co-axial reagent. When the valve is closed, self-coupling hydrazine reactions are facilitated. When the valve is opened, the full capacity of the programmable platform is realized by allowing cross-coupled products. A direct current (DC) high voltage is applied directly to the etched silica capillary at 6 kV allowing simultaneous generation of plasma discharge during the evolution of charged microdroplet.[9,63] Further details on emitter optimization and experimental setup are provided in Supporting Information, **Figures S1**–**S3**. High energy electrons within plasma interact with hydrazine substrate to yield analogous radical intermediate species shown in Figure 1B, which subsequently merge in the charged microdroplet environment to yield the secondary amine coupling product in real-time. Reaction programmability is achieved via the identity of species sprayed from the etched (plasma-microdroplet) and fused (microdroplet only) silica capillaries. Additional

reaction programmability is achieved via the configurable outlet of the platform displayed in Figure 1A**i** and **1Aii** with two distinct operational modes based upon the combination of inner co-axial spray capillaries and an outer concentric capillary of larger diameter. Type I spray mode occurs when the co-axial inner capillaries protrude from the concentric outer capillary thus giving microseconds timescale reactivity.[64] The Type II spray mode occurs when the co-axial inner capillaries are recessed within the outer capillary, forming a cavity of variable length that allows milliseconds-seconds timescale reactivity based upon the size of the reaction cavity and the speed of the droplets, which is dictated by the pressure of the nitrogen nebulizing gas.[65] Type I mode is characterized by short droplet lifetime, droplet-phase mixing, whereas Type II mode is characterized by extended lifetime of reaction species, due to the presence of both droplets and discontinuous thin film, facilitated by the turbulence mixing occurring inside the outer capillary. Additional details on operational mode characteristics is provided in the Supporting Information.

Figure 1B shows the general reaction mechanism proposed for the uncatalyzed, radical mediated coupling of hydrazines. The experimental evidence of this mechanism is provided in Figure 1C, where signal for the radical intermediate as well as the secondary amine product were monitored over the course of a voltage-ion current study measured by MS. The important role of spray voltage is observed here, where the absolute abundance of intermediate and product species both increased as a function of voltage. This is attributable to plasma-microdroplet operation where higher voltage induces a stronger electric field across the sharpened tip of the etched silica emitter via the relation $E = V/m$ where E is the electric field, V is the applied voltage, and m is the radius of curvature of the conductive etched emitter (~100 μm).[9] Therefore, as applied voltage increases, so does the magnitude of the electric field, inducing greater abundance of homolytic cleavage intermediates, which are subsequently captured by charged microdroplets for real-time coupling to afford the secondary amine product. This plasma-over-water reaction condition is ideal for product formation due to reactant sequestration in the charged microdroplets—a feat challenging for pure gas-phase plasma systems.[53] Additional mechanistic studies are outlined below, which investigate i) the effect of solvent on the formation of radical intermediate and final secondary amine product and ii) the effect of the tunable parameters of the co-axial platform (i.e. reagent volumetric flowrate, applied voltage, nitrogen nebulizer gas pressure, and cavity size used in Type II spray mode (**Figure S1–S3**).

Uncatalyzed Radical Mediated Hydrazine Self-Coupling

To investigate the ability of the plasma-microdroplet fusing platform to perform uncatalyzed radical mediated hydrazine coupling, we first studied a series of structurally diverse hydrazine substrates independently and evaluated their self-coupling products. We employed electron rich and electron poor substrates sprayed using both Type I and Type II operation modes. We also investigated the resultant reactions in both positive- and negative-ion modes for both spray mechanisms (i.e., Types I and II). First, we evaluate the effect of operational mode on electron rich versus electron poor substrates in Figure 2 using three independent phenylhydrazine substrates: 4-methoxyphenylhydrazine (MW 138 Da) as an electron-rich substrate, 4-nitrophenylhydrazine (MW 154 Da) as an electron-poor substrate, and phenelzine (MW 136 Da) as an electron-neutral substrate with the hydrazine moiety located two carbons away from the benzene ring. Interestingly, a distinct reaction timescale effect is observed for electron rich versus electron poor substrate. The electron rich 4-methoxyphenylhydrazine self-coupling product (MW 229 Da) is observed in Type I, microseconds timescale (droplet speed ~120 m/s, spray distance 2 mm)[64] operation as a protonated pseudomolecular ion in positive-ion mode (Figure 2A). On the other hand, the electron poor 4-nitrophenylhydrazine self-coupling product (MW 259 Da) required longer timescale, which was achieved in Type II operation offering seconds reaction time due to the presence of the cavity.[65] In this case, the 4-nitrophenylhydrazine self-coupling product was observed as a radical anion in negative-ion mode (Figure 2B). The effect of ionization polarity will be discussed later. Interestingly, the electron-neutral phenelzine substrate gave a dehydrogenated radical cation product (common in plasma chemistry due to the presence of hydrogen abstracting species)[9,60] (MW 223 Da) in Type I operational mode—thus microsecond timescale is sufficient for the coupling reaction

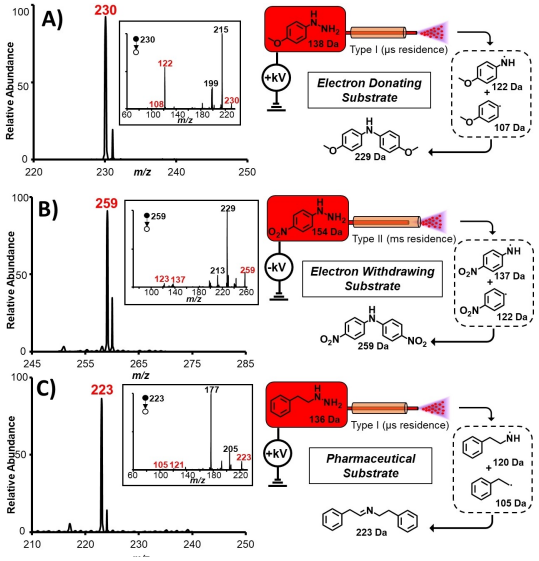

Figure 2. Investigation of electronic effects on hydrazine self-coupling with **A**) electron-rich 4-methoxyphenylhydrazine substrate analyzed in Type I mode with protonated $[M+H]^+$ product in positive-ion mode and inset MS/MS showing diagnostic radical intermediate ions, **B**) electron-poor 4-nitrophenylhydrazine substrate sprayed in Type II mode with electron capture $[M]^{-\bullet}$ product in negative-ion mode and inset MS/MS showing diagnostic radical intermediate ions, and **C**) electron-neutral phenelzine substrate analyzed in Type I mode with dehydrogenated radical cation $[M]^{+\bullet}$ product formation and inset MS/MS showing diagnostic radical intermediate ions.

devoid of any electronic penalty (Figure 2C). All products were validated directly via tandem MS (MS/MS) performed online, since the reaction platform acts as an ionization source for mass spectrometry. MS/MS spectra are shown as inset for Figure 2A**–2C**, and show distinct dissociation pathways giving rise to the expected diagnostic fragment ions (shown in red for the inset spectra) for each reaction. The fragment ion at *m/z* 122 in the insert of Figure 2A is unique in that it is a radical cation, which might be formed from a complicated rearrangement process involving homolytic cleavage of C–N bond followed by hydrogen atom transfer to form a neutral anisole (MW 108 Da) compound.

Full mass spectra in a wider mass range are displayed in **Figure S4A**–**S4C** for these reactions. Controls experiments demonstrating the importance of reaction timescale were investigated for these reactions. That is, using an etched silica capillary, we study the reactivity of 4-methoxyphenylhydrazine in Type II mode on seconds time scale (optimized spray condition was the microsecond Type I spray mode), 4-nitrophenylhydrazine and phenelzine in Type I and in Type II modes, respectively, which are not the optimized spray conditions (see Supporting Information **Figure S5** for details). The yield for 4-methoxyphenylhydrazine coupling was decreased in Type II mode (**Figure S5A**), 4-nitrophenylhydrazine coupling was also decreased in Type I mode (**Figure S5B**), as well as the yield phenelzine coupling in Type II mode (**Figure S5C**). Again, these are compared to optimized spray conditions discussed in Figure 2 for the etched capillary. These results demonstrate that the spray mode, and reaction timescale, are crucial for these radical mediated coupling reactions and should be optimized for each species, thus requiring the programmability discussed later in this work. For example, extended confinement of plasma species in the charged microdroplet environment can lead to neutralization of active species, which lead to reduced yield for some substrates. For other species, however, extended reaction time is required to convert substrate to the desired product. Additional controls were performed using a microdroplet-only c-ESI platform, which was fitted with fused silica capillaries. We observed null product formation in both Type I microdroplet-only (**Figure S6**) and Type II microdroplet-only spray modes (**Figure S7**) of the platform. These results demonstrate the importance of nonthermal plasma in the spray process for the coupling reaction.

Electroneutrality Effect on Coupling Reactions

Plasma formation is known to be independent of voltage polarity. Therefore, we expected product formation in both positive- and negative-ion modes. This effect can be studied using substrates capable of both protonation (positive-ion mode) and electron capture (negative-ion mode) ionization mechanisms. For example, this effect was observed for 4-nitrophenylhydrazine (MW 154 Da) in Figure 2B (also see **Figure S5B**) where unreacted reagent (*m/z* 154) and expected coupling product (*m/z* 259) were detected as radical anions through electron capture in the negative spray mode. To fully explore the electroneutrality of plasmas and their ability to induce radical-mediated hydrazine coupling irrespective of polarity of voltage applied, we further evaluated three independent phenylhydrazine substrates: 4-chlorophenylhydrazine (MW 142 Da), 4-bromophenylhydrazine (MW 186 Da), and phenylhydrazine (MW 169 Da), representing two electronegative and one electroneutral substrate, respectively.

The results of this investigation are shown in Figure 3 where full mass spectra are displayed for both positive- (Figures 3B, **3E**, and **3H**) and negative- (Figures 3C, **3F**, and **3I**) spray modes. The analogous larger range full mass spectra are provided in the Supporting Information **Figure S8** with positive-ion (**Figure S8B, S8E**, and **S8H**) and negative-ion products (**Figure S8C, S8F**, and **S8I**). Interestingly, negative-ion spray mode gave higher relative abundance of product species (**Figure S8**). We attribute this effect to two related effects: i) the enhanced potency of negative-ion mode plasma where electron generation is enhanced since electrons are the negative charge carriers and initiators of the reaction, and ii) the electronegativity of the substituted 4-chloro and 4-bromo groups, which makes their electron capture ionization efficiency better than the corresponding protonation, and thus yielding higher ion current in negative-ion mode. Figure 3A shows reaction platform (Type I mode, microseconds timescale) and reaction Scheme for the self-coupling reaction of 4-chlorophenylhydrazine yielding the secondary amine product (MW 237 Da). Figure 3B shows positive-ion mode operation for 4-chlorophenylhydrazine showing protonated coupling product. Note: the characteristic chlorine isotopic ratio gives protonated product peaks at *m/z* 238 and 240. Inset MS/MS of the product show diagnostic fragmentation giving radical intermediate species. Figure 3C shows negative-ion mode spray of the same 4-chlorophenylhydrazine, which now shows radical anions of expected coupling product, with isotopic peaks at *m/z* 237 and 239. Inset MS/MS of the product again shows diagnostic fragmentation giving expected radical intermediate species. Figure 3D shows reaction platform (Type II mode, seconds timescale) and reaction scheme for the self-coupling reaction of 4-bromophenylhydrazine yielding the corresponding secondary amine product (MW 325 Da). Figure 3E shows the positive-ion mass spectrum recorded after spraying 4-bromophenylhydrazine with the c-ESI source, in the presence of cavity. We observed the protonated reaction product, with characteristic bromine isotopic ratio at *m/z* 326, 328 and 330. Inset MS/MS of the product show diagnostic fragmentation giving radical intermediate species. Figure 3F shows negative-ion spectrum for 4-bromophenylhydrazine, showing radical anions of the expected secondary amine, with isotopic peaks at *m/z* 325, 327 and 329. Here too, the inset MS/MS shows diagnostic fragmentation giving expected radical intermediate species. Lastly, we studied the self-coupling reaction of phenylhydrazine in both positive- and negative-ion modes using the platform shown in Figure 3G (Type II mode, seconds reaction time). Figure 3H shows positive-ion mode analysis of phenylhydrazine indicating protonated self-coupling product at *m/z* 170, together with the radical cation at *m/z*

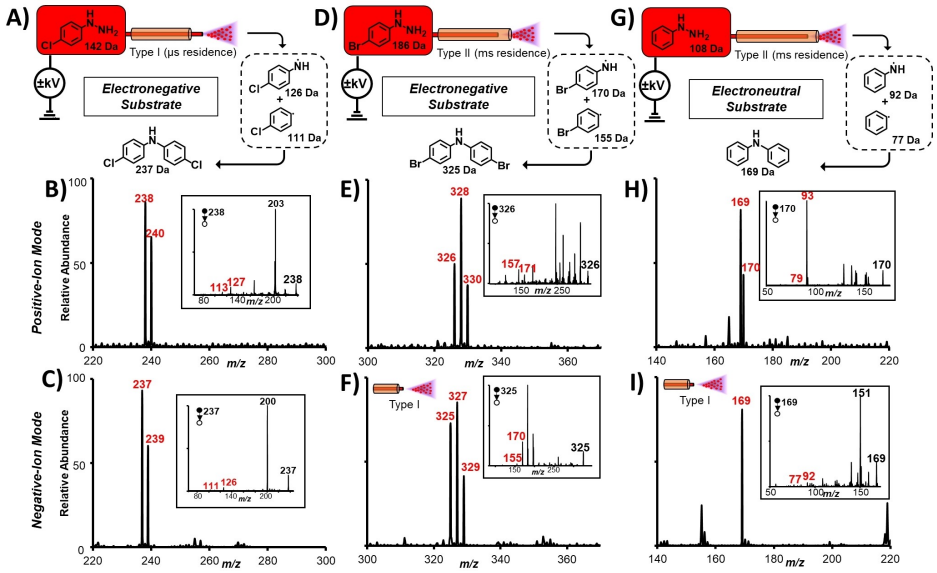

Figure 3. Investigation of platform polarity on hydrazine coupling with **A**) reaction platform setup and reaction scheme for 4-chlorophenylhydrazine self-coupling, **B**) positive-ion mode operation of 4-chlorophenylhydrazine showing protonated product with inset MS/MS, **C**) negative-ion mode operation of 4-chlorophenylhydrazine showing electron capture product with inset MS/MS, **D**) reaction platform setup and reaction scheme for 4-bromophenylhydrazine self-coupling, **E**) positive-ion mode operation of 4-bromophenylhydrazine showing protonated product with inset MS/MS, **F**) negative-ion mode operation of 4-bromophenylhydrazine showing electron capture product with inset MS/MS (note: Type I operational mode was used in negative-ion mode), **G**) reaction platform setup and reaction scheme for phenylhydrazine self-coupling, **H**) positive-ion mode operation of phenylhydrazine showing protonated product with inset MS/MS, **I**) negative-ion mode operation of phenylhydrazine showing electron capture product with inset MS/MS (note: Type I operational mode was used in negative-ion mode).

169. The inset MS/MS of ions at *m/z* 170 $[M+H]^+$ shows diagnostic fragmentation giving radical intermediate species. Figure 3I shows negative-ion mode analysis of the same phenylhydrazine reagent but in this case the predominant species detected is at *m/z* 169, which corresponds to radical anion of the expected product following electron capture ionization.

Again, we confirmed the structure of this product via MS/MS analysis, shown as inset in Figure 3I. Interestingly, the self-coupling products of 4-bromophenylhydrazine and phenylhydrazine were observed in high yields when utilizing Type II spray mode for positive plasma (Figures 3E and **3H**). However, the short timescale Type I spray mode was required to generate the same self-coupling products from the same reagents (bromophenylhydrazine and phenylhydrazine) when negative plasma was used (Figures 3F and **3I**). These results suggest an enhanced potency for negative plasma (due to higher electron density) for hydrazine coupling. But, our reaction platform is able to compensate for the reduced energy in positive plasma by allowing extra time for reaction by operating the platform in Type II mode. For all reactions discussed in Figure 3, the opposite emitter operational modes were also applied in an attempt to confirm the effect of time scale on hydrazine coupling under the plasma-microdroplet fusion experimental condition. For example, Type II mode analysis of 4-chlorophenylhydrazine in positive plasma showed no coupling product (**Figure S9A**) but the Type I spray mode produced abundant products (Figure 3B). Results for the other reagents tested are summarized in **Figure S9**. In all cases, the desired product is either reduced or non-existent under non-optimal programming condition, which emphasize the importance of reaction timescale for product programming. Aside from the necessity to control reaction time, the type of capillary used is also important, as already demonstrated in Figure 2. That is, the use of fused silica capillary provides an important control to confirm the importance of plasma in this hydrazine coupling reaction. As expected, this microdroplet-only experiment performed with fused silica capillaries produced null coupling product because of the absence of non-thermal plasma discharge (**Figure S10**).

Benzylhydrazine Substrates for Aryl-Aldimine Syntheses

Having established that the presence of non-thermal plasma and timescale of reaction in the microdroplet environment are important parameters, we sought to expand the scope by using benzylhydrazine substituents (instead of phenylhydrazine substituents discussed above) for the synthesis of aryl-aldimines. Substituted aryl-aldimines are important organic moieties with enzymatic and pharmaceutical interests as they exhibit anti-cancer and anti-fungal properties.[41–43] The secondary amine coupled product from benzylhydrazines represents a structural precursor to aryl-aldimine synthesis. Note: cross-coupling of benzylhydrazines leads to a more clinically relevant aryl-aldimines, but we discuss the self-coupling process first. Figure 4A shows the positive-ion mode mass spectrum derived from spaying 4-bromobenzylhydrazine under Type I plasma-microdroplet conditions

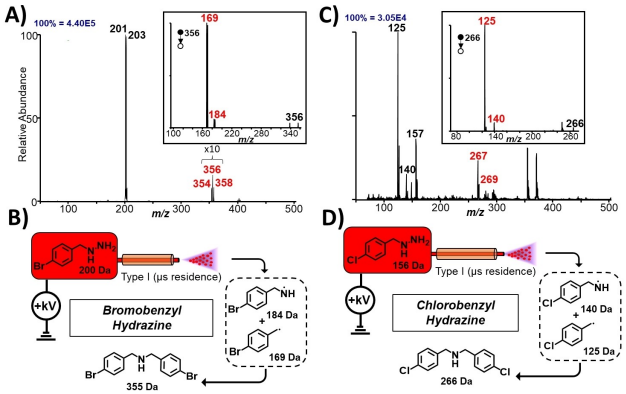

Figure 4. Benzylhydrazine self-coupling reactions with **A**) 4-bromobenzylhydrazine producing protonated secondary amine, inset MS/MS shows fragmentation yielding radical intermediate ions, **B**) reaction platform operation and reaction scheme for 4-bromobenzylhydrazine self-coupling, **C**) 4-chlorobenzylhydrazine self-coupling to give protonated secondary amine, inset MS/MS shows fragmentation yield radical intermediate ions, and **D**) reaction platform operation and reaction scheme for 4-chlorobenzylhydrazine self-coupling.

where the secondary amine product peaks are observed at *m/z* 354, 356, and 358 as protonated species.

These correspond to the expected di-bromine isotopic ratio pattern found in the self-coupled reaction product. The inset in Figure 4A shows the MS/MS at *m/z* 356 where diagnostic fragmentation ions are observed in the form of the radical intermediates. Figure 4B shows the reaction platform along with the corresponding reaction scheme for 4-bromobenyzlhydrazine self-coupling. Similarly, chlorobenzylhydrazine was analyzed using the platform shown in Figure 4D (Type I operation mode), with the corresponding mass spectrum shown in Figure 4C. The expected secondary amine self-coupling products are detected at *m/z* 267 and 269, corresponding to the expected di-chlorine isotopic ratio pattern. Here too, MS/MS analysis confirmed structure by giving rise to diagnostic fragments in the form of radical cation intermediates. Control experiments were performed for both chemical systems using a c-ESI setup fitted with deactivated fused silica capillaries. Null product formation was observed in the absence of plasma discharge—again pointing to the importance of electron collisions for facilitating this radical-mediated coupling reaction.

Dehydrogenation of the secondary amines derived from coupling of benzylhydrazines give rise to the aryl-aldimine derivatives we seek. To achieve this objective, we altered the reaction platform by changing the timescales of the plasma-microdroplet fusion process to enable the formation of the dehydrogenated product. We expected the online dehydration to be possible because of the hydrogen abstraction capacity of plasma discharge due to the reactive oxygen species such as $O_2^{\bullet-}$. The results of this investigation are available in Supporting Information, **Figure S11**. **Figure S11A** describes the self-coupling of 4-bromobenzylhydrazine to give bis(4-bromobenzyl)amine (MW 355 Da) followed by dehydrogenation to afford the corresponding imine (MW 353 Da), which was subsequently detected as protonated species at *m/z* 354. Notice how the product distribution has shifted from clean secondary amine formation (Figure 4A) to aldimine production (**Figure S11A**) simply by changing timescale of the plasma-microdroplet fusion process, from microseconds (Type I mode) to seconds (Type II mode) reaction timescales. Similar observation was reproduced for 4-chlorobenzylhydrazine in **Figure S11C** after analyzing it Type II spray mode, with the corresponding final dehydrogenated aldimine product detected product at *m/z* 265. These reactivities were achieved using etched silica capillaries. We performed control experiments utilizing fused silica capillaries, which allowed both bromobenzylhydrazine and chlorobenzylhydrazine to be studied separately under charged microdroplet-only conditions without the emergence of nonthermal plasma. Null product formation was observed for both reagents in the absence of plasma (**Figure S12**).

Programmable Cross-Coupling Reactions

The overarching objective of this study was to synthesize pharmaceutically relevant compounds through cross-coupling of hydrazine to produce secondary amines and aryl-aldimines having two unique N-substitutions. We envisioned that the use of co-axial plasma-microdroplet fusing platform illustrated in Scheme 1B will enable us to program the synthesis of specific species and avoid other reaction pathways. Such an endeavor will be challenging to achieve using the traditional one-pot electrospray platform (Scheme 1A). The actual implementation of the co-axial platform is illustrated in Figure 1A, with the valve in blue fused silica capillary opened. The programmable features of this co-axial platform are illustrated in Scheme 2A, which include the control of spray capillary type, reaction timescale, and reagent concentration. Through the investigation of six unique hydrazine substrates, we identified the six corresponding self-coupling products (i.e., R_1=R_2 in Scheme 2A). Similarly, using the same six hydrazine substrates, we synthesized six unique cross-coupling products (i.e., $R_1 \neq R_2$ in Scheme 2A), which are identified to be relevant to pharmaceutical development.[41] Interestingly, each unique cross-coupled product required a unique set of spray conditions, which were easily programmed using the co-axial spray platform as described in Figure 5.

Figure 5 summarizes the programs used for the co-axial plasma-microdroplet fusing platform for selective product synthesis of specific products. Proper capillary selection allows specific reagents to be activated in plasma (etched silica capillary) or not (fused silica capillary). Reagent flow rates in the respective capillaries set the corresponding reagent concentration used in the reaction. Reagent flow rate <5 µL/min is considered low whereas reagent flow rate >5 µL/min is considered high. The third controllable parameter, besides capillary type and flowrate, is related to reaction timescale, which is programmed by selecting the mode of operation of the c-ESI platform. As already demonstrated, the Type I operation mode allows faster (microseconds) timescale of reactions in the microdroplet

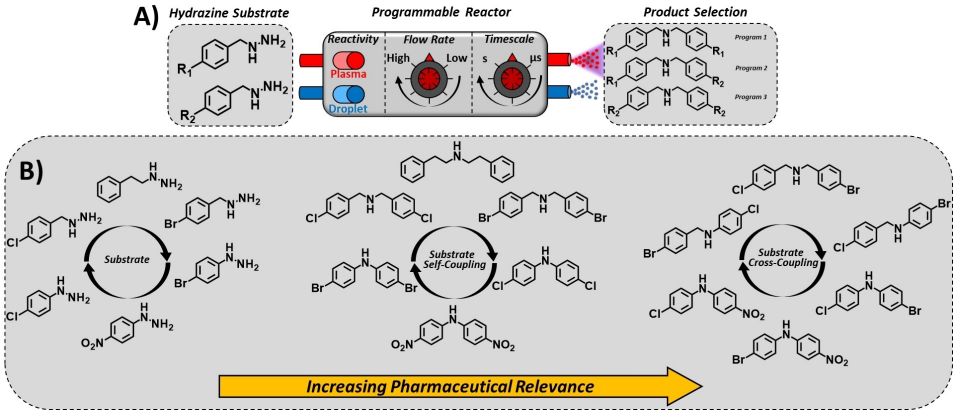

Scheme 2. **A**) Programmable plasma-microdroplet reaction platform for the production of structurally heterogeneous cross-coupled products. **B**) Hydrazine substrates evaluated including self-coupling reaction products and cross-coupling reaction products, where cross-coupled species are of greater pharmaceutical relevance.

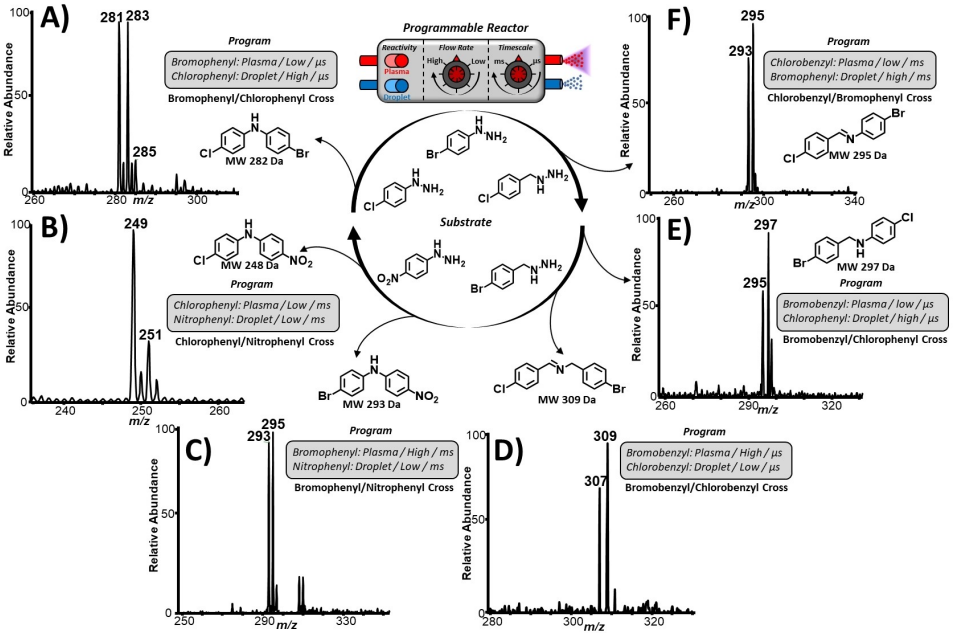

Figure 5. Programmable cross-coupling reactions via plasma-microdroplet fusion with **A**) 4-bromophenylhydrazine/4-chlorophenylhydrazine cross-coupling reaction, **B**) 4-chlorophenylhydrazine/4-nitrophenylhydrazine cross-coupling reaction, **C**) 4-bromophenylhydrazine/4-nitrophenylhydrazine cross-coupling reaction, **D**) 4-bromobenzylhydrazine/4-chlorobenzylhydrazine cross-coupling reaction giving the dehydrogenated product, **E**) 4-bromobenzyllhydrazine/4-chlorophenylhydrazine cross-coupling giving the cross-coupling product (precursor to the dehydrogenated aryl-aldimine product), and **F**) 4-chlorobenzylhydrazine/4-bromophenylhydrazine cross-coupling followed by dehydrogenation to give the aryl-aldimine product.

environment while the Type II mode of operation offers longer (seconds) reaction time. Figure 5A shows the cross-coupling reaction between 4-bromophenylhydrazine and 4-chlorophenyl hydrazine to give cross product, 4-bromo-N-(4-chlorophenyl)aniline (MW 282 Da), which is detected as radical anion via electron capture ionization in negative-ion mode. This product was programmed by spraying 4-bromophenylhydrazine through the plasma inducing capillary at low flow rate in Type I operation (microseconds timescale) while also spraying 4-chlorophenylhydrazine from the microdroplet-only capillary at high flow rate in Type I operation. Collectively, these conditions specifically favor the cross-coupling product over both the 4-chloro and 4-bromo self-coupling products alone. Figure 5B shows spray conditions for selectively synthesizing the cross-coupled reaction product, 4-chloro-N-(4-nitrophenyl)aniline (MW 248 Da) from 4-nitrophenylhydrazine and 4-chlorophenyl hydrazine. This product is observed as protonated species at *m/z* 249 in positive-ion mode with the expected 3:1 ^{37}Cl:^{35}Cl isotopic ratio. The specific program used include spraying 4-nitrophenylhydrazine through the microdroplet-only fused silica capillary at low flow rate in Type II operation (seconds timescale) while concomitantly spraying 4-chlorophenylhydrazine from the plasma etched silica

capillary at low flow rate, also in Type II mode. Combined, these conditions favored the cross-coupling product specifically over both the 4-chloro and 4-nitro self-coupling products alone.

Figure 5C shows the synthesis of 4-bromo-N-(4-nitrophenyl)aniline (MW 293 Da), which is the cross-coupled reaction product between 4-nitrophenylhydrazine and 4-bromophenyl hydrazine. We detected 4-bromo-N-(4-nitrophenyl)aniline as protonated pseudomolecular ion in positive-ion mode with expected bromine isotopic ratio. This product was programmed by spraying 4-nitrophenylhydrazine through the microdroplet-only fused silica capillary at low flow rate using Type II operation (seconds timescale) while delivering 4-bromophenylhydrazine from the plasma etched silica capillary at high flow rate, also in Type II operation mode. As shown, these conditions specifically favor the cross-coupling product over both the 4-bromo and 4-nitro self-coupling products alone. Likewise, Figure 5D shows how the aryl-aldimine compound, (E)-N-(4-bromobenzyl)-1-(4-chlorophenyl)methanimine (MW 309 Da), was synthesized through the cross-coupling reaction between 4-bromobenzylhydrazine and 4-chlorobenzylhydrazine. This reaction first affords the secondary amine N-(4-bromobenzyl)-1-(4-chlorophenyl)methanamine (MW 311 Da), which subsequently undergoes dehydrogenation via H_2 loss, a phenomenon common in plasma discharge.[9,60] This cross-coupled aryl-aldimine product was detected as radical anion via electron-capture ionization in negative-ion mode with expected chloro/bromo isotopic ratio. This product was programmed by spraying 4-bromobenzylhydrazine through the plasma capillary at high flow rate in Type I operation (μs timescale) while also spraying 4-chlorobenzylhydrazine from the fused silica microdroplet-only capillary at low flow rate in Type I mode of operation. As discussed above, these conditions interestingly favored the dehydrogenated cross-coupled product over other possible species. Lastly, Figures 5E and **5F** display particularly interesting chemical systems in the cross coupling reaction of 4-bromobenzylhydrazine and 4-chlorophenylhydrazine in Figure 5E and 4-chlorobenzylhydrazine and 4-bromophenylhydrazine in Figure 5F. The cross-coupled secondary amine products of these two systems have an identical mass (MW 297 Da), differing only by the fact that reaction conditions are programmed such as one of the secondary amines undergoes dehydrogenation to give the corresponding aryl-aldimine functional group (MW 295). Here, platform program yielding the cross-coupled secondary amine is shown in Figure 5E and the program resulting in the dehydrogenated (aryl-aldimine) product is shown in Figure 5F. The specific cross-coupling reaction program for producing the secondary amine, N-(4-bromobenzyl)-4-chloroaniline, involves spraying the bromobenzyl substituent through the plasma capillary at low flow rate and in Type I mode (μs timescale). At the same time, we sprayed the chlorophenyl substituent from the microdroplet-only fused silica capillary at high flow rate and in Type I mode of operation. The synthesis of the dehydrogenated aryl-aldimine product, (E)-N-(4-bromophenyl)-1-(4-chlorophenyl)methanimine, was achieved under Type II operational mode (seconds timescales), where the chlorobenzyl substituent was sprayed via plasma capillary at low flow rate while the bromophenyl substituent was sprayed via the microdroplet-only fused silica capillary at high flow rate. Again, both sprays occurred in Type II operation mode where the longer reaction time available in this mode makes it possible to complete this multi-step reaction mechanism, in the microdroplet environment: homolytic cleavage, followed by coupling of specific radical intermediates to give the secondary amine, and finally dehydrogenation of the amine to give the corresponding aryl-aldimine by the action of reactive oxygen species.

Structural analyses for all cross-coupled products were performed via direct MS/MS, with the corresponding product-ion scans for the six products shown in the Supporting Information, **Figure S13**. Herein all fragmentation patterns were consistent with previous MS/MS interpretation whereby the radical intermediates are observed as the diagnostic fragment ions for all cross-coupled products. See Supporting Information for details. To complete this aspect of the work, we performed supporting controls, which include i) evaluation of programming selectivity over a wider mass range in the full mass spectrum (**Figure S14A–F)** for all chemical systems studied in Figure 5A–**F**, and ii) changing the spray parameters for product programmability in terms of the formation of dehydrogenated (i.e., aryl-aldimine) versus non-dehydrogenated (i.e., secondary amine) species as shown in **Figure S15**.

Microdroplet-Based Borsche–Drechsel Cyclization and the Effect of Reaction Programmability

We conclude this investigation with an application of the programmable platform to a cascade cyclization reaction, which also relies on C–N bond formation. In this case, our goal is to avoid homolytic cleavage of hydrazine whilst also facilitating its reaction in the charged microdroplet environment. For this, we used the Borsche-Drechsel (B–D) cyclization reaction. The B–D reaction represents an important synthetic step in the formation of heterocyclic carbazole derivatives, which have ubiquitous pharmacological importance.[66,67] Traditional bulk-phase synthesis requires boiling sulfuric acid and extended reaction times. Efforts towards more sustainable B–D cyclization have included the use of ionic liquids, toluenesulfonic acid in solvent free conditions, zeolite catalysis, and tartaric acid/dimethyl urea catalysis.[67–69] Here again, we seek the opportunity to achieve green synthesis via catalyst-free plasma discharge.

B–D cyclization involves Schiff base formation between cyclohexanone (MW 98 Da) and a substituted phenylhydrazine. A significant thermodynamic barrier to cyclization must then be overcome for the final heterocyclic B–D product, 4-substituted carbazole, to form. Scheme 3 shows the general methodology for the use of the programmable plasma-microdroplet fusion platform for B–D cyclization. Again, the co-axial spray platform facilitates selective product programming and avoids side products via proper reagent-capillary matching. For instance, hydrazine self-

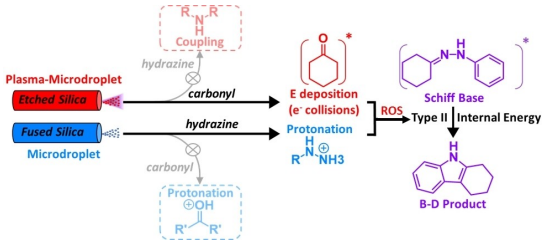

Scheme 3. General schematic for the use of the programmable co-axial plasma-microdroplet reaction platform for B–D cyclization through programming both by reagent/capillary selection and by reaction timescale.

coupling, which is a side reaction in this case, can be avoided by spraying the hydrazine reagent through the microdroplet-only fused silica capillary. Under this spray condition, the hydrazine forms only protonation species in positive-ion mode. On the contrary, spraying the hydrazine through the etched silica capillary will result in self-coupling to form secondary amine as demonstrated earlier in this study. Similarly, spraying the cyclohexanone through the fused silica capillary leads only to protonation. However, when sprayed through the etched silica capillary, cyclohexanone is expected to gain internal energy because of the presence of high energy collisions in nonthermal plasma, thus resulting in an activated cyclohexanone which can be expected to react more favorably in subsequent reaction steps when the conditions are right. Therefore, the Schiff base formation between hydrazine and cyclohexanone may then proceed more efficiently in the plasma-microdroplet fusion environment. The reactive oxygen species present in the plasma may further facilitate the Schiff-base formation by abstracting protons from the protonated hydrazine delivered by the fused silica, thus freeing the lone pair of electrons in the hydrazine for nucleophilic attack on the activated cyclohexanone. By providing sufficient time in Type II spray mode, we expected the cyclization step leading the formation of the final 4-substituted carbazole to be favored and straightforward (Scheme 3).

This methodology was applied to synthesize three unique 4-substituted carbazole derivatives through the reaction of three different hydrazine reagents with cyclohexanone. The hydrazines substrates tested included: 4-methoxyphenylhydrazine, phenylhydrazine, and 4-nitrophenylhydrazine. These reagents were selected to offer electron-donating and electron-withdrawing effects. The results of these investigations are shown in Figure 6, all of which utilized an identical reaction program (Figure 6A) where cyclohexanone reagent was sprayed through the etched silica capillary (presence of plasma) while the hydrazine reagent was sprayed from the fused silica capillary (microdroplet-only), both at low flow rate using the Type II operations mode (seconds timescale). The result from reaction between cyclohexanone and 4-methoxyphenylhydrazine is described in Figure 6B where the Schiff base intermediate formation is observed as a protonated ion at *m/z* 219 and the final carbazole B–D product detected as protonated species at *m/z* 202. As can be observed, close to 90 % of the hydrazine (observed at *m/z* 139 in Figure 6B) sprayed from the fused silica is converted into the Schiff base, and >30 % of the Schiff base is in turn converted into the final cyclized product. Similarly, the B–D cyclization reaction between phenylhydrazine and cyclohexanone is shown in Figure 6C

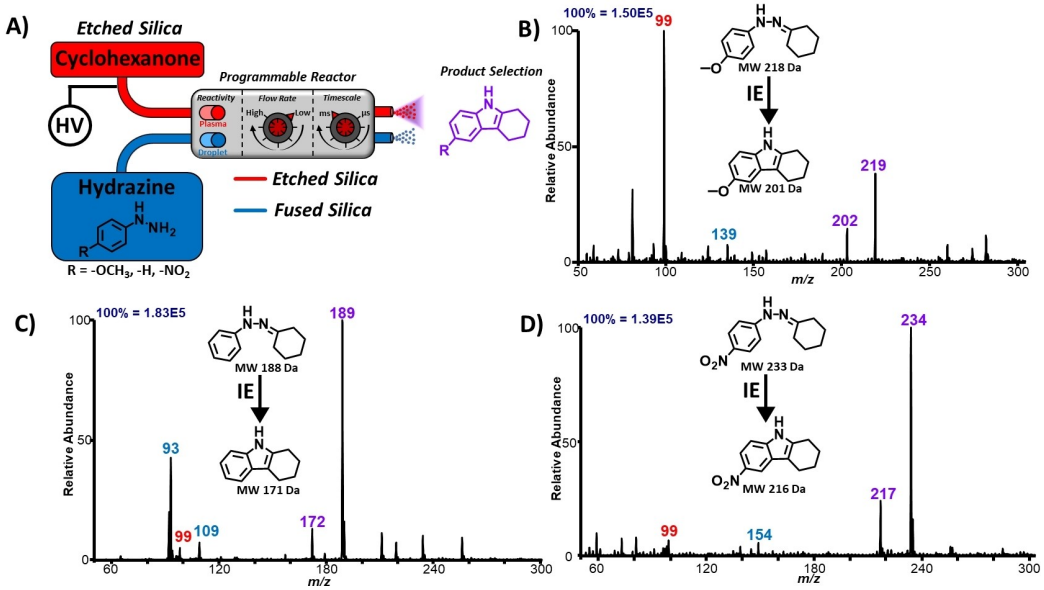

Figure 6. Programmable B–D Cyclization via plasma-microdroplet fusion with **A**) platform operational programming with cyclohexanone introduction via etched silica and hydrazine reagent introduction via fused silica both under low flow rate and second (Type II) timescale programming. **B**) B–D cyclization between cyclohexanone and 4-methoxyphenylhydrazine giving the methoxy-substituted carbazole at *m/z* 202. **C**) B–D cyclization between cyclohexanone and phenylhydrazine giving the unsubstituted carbazole at *m/z* 172. **D**) B–D cyclization between cyclohexanone and 4-nitrophenylhydrazine giving the nitro-substituted carbazole at *m/z* 217.

where the protonated Schiff base intermediate is observed at *m/z* 189 and the corresponding carbazole B–D product is observed at *m/z* 172. Here too, >90 % of the sprayed hydrazine (detected at *m/z* 109 in Figure 6C) was converted into the Schiff base in real-time. In this case, we observed some homolytic cleavage of the hydrazine, but the self-coupling product is absent (expected MW 169 Da). Instead, about 10 % of the Schiff base was converted to the final carbazole product, detected at *m/z* 172 in Figure 6C. Finally, Figure 6D shows the B–D cyclization reaction between 4-nitrophenylhydrazine and cyclohexanone, where the protonated Schiff base intermediate is again observed as a base peak at *m/z* 234 and the carbazole B–D product is observed at *m/z* 217. Here, about 95 % of hydrazine sprayed was converted into the corresponding Schiff base, of which ~20 % went on to produce the final carbazole product. These conversion ratios represent one of the highest yields reported for cascade reactions under the charged microdroplet environment.[9,12,21,70,71] We did not observe significant electronic effects under the plasma-microdroplet fusion reaction condition as both electron-rich and poor-substrate performed well. This supports the understanding that the rate-limiting step for this reaction is indeed the thermodynamic barrier to cyclization step and not the initial Schiff base formation. Structural evidence for the Schiff base intermediate and carbazole products is provided in the Supporting Information through MS/MS analysis in **Figure S16**. All species showed fragmentation patterns characteristic of the expected structure.

A fundamental investigation of the effect of voltage on all reactions studied herein was performed, with results summarized in **Figures S17–S21** as well as the accompanying discussion provided in the Supporting Information. Additionally, reaction yields, product enhancement factors of plasma-microdroplet operation versus microdroplet-only controls, and reaction reproducibility studies were performed and are discussed in the Supporting Information for all twenty reactions studied in **Tables S1–S6**, and **Equation S1**. The main limitation of the current method include the use of low reagent flow rates, which can reduce overall yield. See Supporting Information discussions on chemical scope and related limitations.

Conclusions

A programmable reaction platform is presented herein for the selective formation of structurally heterogeneous cross-coupled products in the charged water microdroplet regime. A co-axial plasma-microdroplet fusion platform is utilized for i) the uncatalyzed radical mediated hydrazine coupling of a wide range of structurally diverse hydrazine substrates, ii) programmable cross-coupling reactions facilitating online selectivity for heterogeneous cross-products by programming reagent/capillary selection and tunable platform parameters including volumetric flow rate and reaction timescale, and iii) formation of substituted carbazole derivatives via B–D cyclization cascade reactions in the green medium of charged water microdroplets. The platform presented herein is the topic of ongoing research toward unique chemical systems, expecting to open new doors for unique reactions in the charged microdroplet environment as well as to create opportunities for large-scale product collections. The application of dicovered reactions in quantitative chemical analysis by mass spectrometry is also being pursued.

Acknowledgements

This research was supported by the U.S. Department of Energy, Office of Basic Energy Sciences, Condensed Phase and Interfacial Molecular Science, under award number DE-SC0022097. MS and LT were supported by the spectroscopy REU program at Ohio State funded by the National Science Foundation (CHE-2150102)

Conflict of Interest

The authors declare no conflict of interest.

Data Availability Statement

The data that support the findings of this study are available in the supplementary material of this article.

Keywords: Analytical methods · Selective radical chemistry · programmable reaction · microdroplet chemistry · Hydrazine cross-coupling

[1] M. Yan, J. C. Lo, J. T. Edwards, P. S. Baran, *J. Am. Chem. Soc.* **2016**, *138*, 12692–12714.
[2] N. K. McMillan, J. Wortley, K. Nguyen, D. A. Lopez, G. Leem, B. D. Sherman, *ACS Appl. Eng. Mater.* **2023**, *1*, 3122–3133.
[3] B. D. Sherman, N. K. McMillan, D. Willinger, G. Leem, *Nano Convergence* **2021**, *8*, 7.
[4] S. Al Zubaydi, I. O. Onuigbo, B. L. Truesdell, C. S. Sevov, *Angew. Chem. Int. Ed.* **2024**, *63*, e202313830.
[5] H. Hintz, J. Bower, J. Tang, M. LaLama, C. Sevov, S. Zhang, *Chem Catal.* **2023**, *3*, 100491.
[6] A. Gupta, J. K. Laha, *Chem. Rec.* **2023**, *23*, e202300207.
[7] E. J. McClain, A. K. Wortman, C. R. J. Stephenson, *Chem. Sci.* **2022**, *13*, 12158–12163.
[8] M. Szwarc, M. G. Evans, *Proc. R. Soc. Lond. Ser. Math. Phys. Sci.* **1949**, *198*, 267–284.
[9] A. J. Grooms, A. N. Nordmann, A. K. Badu-Tawiah, *Angew. Chem. Int. Ed.* **2023**, *62*, e202311100.
[10] R. Augusti, H. Chen, L. S. Eberlin, M. Nefliu, R. G. Cooks, *Int. J. Mass Spectrom.* **2006**, *253*, 281–287.
[11] R. G. Cooks, H. Chen, M. N. Eberlin, X. Zheng, W. A. Tao, *Chem. Rev.* **2006**, *106*, 188–211.
[12] M. Girod, E. Moyano, D. I. Campbell, R. G. Cooks, *Chem. Sci.* **2011**, *2*, 501–510.
[13] A. K. Badu-Tawiah, D. I. Campbell, R. G. Cooks, *J. Am. Soc. Mass Spectrom.* **2012**, *23*, 1461–1468.
[14] Y. Li, Y. Liu, H. Gao, R. Helmy, W. P. Wuelfing, C. J. Welch, R. G. Cooks, *Chem. Eur. J.* **2018**, *24*, 7349–7353.

[15] R. M. Bain, C. J. Pulliam, S. T. Ayrton, K. Bain, R. G. Cooks, *Rapid Commun. Mass Spectrom.* **2016**, *30*, 1875–1878.
[16] X. Yan, R. Augusti, X. Li, R. G. Cooks, *ChemPlusChem* **2013**, *78*, 1142–1148.
[17] R. M. Bain, C. J. Pulliam, F. Thery, R. G. Cooks, *Angew. Chem. Int. Ed.* **2016**, *55*, 10478–10482.
[18] H. Xiong, J. K. Lee, R. N. Zare, W. Min, *J. Phys. Chem. Lett.* **2020**, *11*, 7423–7428.
[19] H. Hao, I. Leven, T. Head-Gordon, *Nat. Commun.* **2022**, *13*, 280.
[20] Y. Li, X. Yan, R. G. Cooks, *Angew. Chem. Int. Ed.* **2016**, *55*, 3433–3437.
[21] S. Banerjee, R. N. Zare, *Angew. Chem. Int. Ed.* **2015**, *54*, 14795–14799.
[22] K.-H. Huang, Z. Wei, R. Graham Cooks, *Chem. Sci.* **2021**, *12*, 2242–2250.
[23] J. K. Lee, D. Samanta, H. G. Nam, R. N. Zare, *Nat. Commun.* **2018**, *9*, 1562.
[24] D. B. Eremin, V. V. Fokin, *J. Am. Chem. Soc.* **2021**, *143*, 18374–18379.
[25] Y. Meng, E. Gnanamani, R. N. Zare, *J. Am. Chem. Soc.* **2023**, *145*, 32–36.
[26] Y. Meng, E. Gnanamani, R. N. Zare, *J. Am. Chem. Soc.* **2022**, *144*, 19709–19713.
[27] L. Qiu, R. G. Cooks, *Angew. Chem. Int. Ed.* **2022**, *61*, e202210765.
[28] J. K. Lee, D. Samanta, H. G. Nam, R. N. Zare, *J. Am. Chem. Soc.* **2019**, *141*, 10585–10589.
[29] D. Gao, F. Jin, J. Kyoo Lee, R. N. Zare, *Chem. Sci.* **2019**, *10*, 10974–10978.
[30] C. Gong, D. Li, X. Li, D. Zhang, D. Xing, L. Zhao, X. Yuan, X. Zhang, *J. Am. Chem. Soc.* **2022**, *144*, 3510–3516.
[31] X. Song, C. Basheer, R. N. Zare, *Proc. Nat. Acad. Sci.* **2023**, *120*, e2301206120.
[32] L. Zhao, X. Song, C. Gong, D. Zhang, R. Wang, R. N. Zare, X. Zhang, *Proc. Nat. Acad. Sci.* **2022**, *119*, e2200991119.
[33] D. Zhang, X. Yuan, C. Gong, X. Zhang, *J. Am. Chem. Soc.* **2022**, *144*, 16184–16190.
[34] T. Wang, Z. Li, H. Gao, J. Hu, H.-Y. Chen, J.-J. Xu, *Chem. Sci.* **2023**, *14*, 11515–11520.
[35] L. Qiu, R. G. Cooks, *Proc. Nat. Acad. Sci.* **2024**, *121*, e2309360120.
[36] D. Xing, Y. Meng, X. Yuan, S. Jin, X. Song, R. N. Zare, X. Zhang, *Angew. Chem. Int. Ed.* **2022**, *61*, e202207587.
[37] Q. Ge, Y. Liu, K. Li, L. Xie, X. Ruan, W. Wang, L. Wang, T. Wang, W. You, L. Zhang, *Angew. Chem. Int. Ed.* **2023**, *62*, e202304189.
[38] Y. Liu, Q. Ge, T. Wang, R. Zhang, K. Li, K. Gong, L. Xie, W. Wang, L. Wang, W. You, X. Ruan, Z. Shi, J. Han, R. Wang, H. Fu, J. Chen, C. K. Chan, L. Zhang, *Chem* **2024**, *10*, 330–351.
[39] K. Gong, J. Ao, K. Li, L. Liu, Y. Liu, G. Xu, T. Wang, H. Cheng, Z. Wang, X. Zhang, H. Wei, C. George, A. Mellouki, H. Herrmann, L. Wang, J. Chen, M. Ji, L. Zhang, J. S. Francisco, *Proc. Nat. Acad. Sci.* **2023**, *120*, e2219588120.
[40] K. Li, W. You, W. Wang, K. Gong, Y. Liu, L. Wang, Q. Ge, X. Ruan, J. Ao, M. Ji, L. Zhang, *Environ. Sci. Technol.* **2023**, *57*, 21448–21458.
[41] J. Lasri, N. E. Eltayeb, S. M. Soliman, E. M. M. Ali, S. Alhayyani, A. Akhdhar, M. A. Hussien, *J. Mol. Struct.* **2023**, *1287*, 135673.
[42] J. S. Bennett, K. L. Charles, M. R. Miner, C. F. Heuberger, E. J. Spina, M. F. Bartels, T. Foreman, *Green Chem.* **2009**, *11*, 166–168.
[43] C. M. da Silva, D. L. da Silva, C. V. B. Martins, M. A. de Resende, E. S. Dias, T. F. F. Magalhães, L. P. Rodrigues, A. A. Sabino, R. B. Alves, Â. De Fátima, *Chem. Biol. Drug Des.* **2011**, *78*, 810–815.
[44] P. Ruiz-Castillo, S. L. Buchwald, *Chem. Rev.* **2016**, *116*, 12564–12649.
[45] S. Hwan Cho, J. Young Kim, J. Kwak, S. Chang, *Chem. Soc. Rev.* **2011**, *40*, 5068–5083.
[46] G. Evano, N. Blanchard, M. Toumi, *Chem. Rev.* **2008**, *108*, 3054–3131.
[47] T. Yan, B. L. Feringa, K. Barta, *Sci. Adv.* **2017**, *3*, eaao6494.
[48] J.-P. Corbet, G. Mignani, *Chem. Rev.* **2006**, *106*, 2651–2710.
[49] M. S. Butler, *Nat. Prod. Rep.* **2008**, *25*, 475–516.
[50] J. Bariwal, E. V. der Eycken, *Chem. Soc. Rev.* **2013**, *42*, 9283–9303.
[51] E. Sperotto, G. P. M. van Klink, G. van Koten, J. G. de Vries, *Dalton Trans.* **2010**, *39*, 10338–10351.
[52] J. Magano, J. R. Dunetz, *Chem. Rev.* **2011**, *111*, 2177–2250.
[53] L. Huang, M. Arndt, K. Gooßen, H. Heydt, L. J. Gooßen, *Chem. Rev.* **2015**, *115*, 2596–2697.
[54] R. N. Salvatore, C. H. Yoon, K. W. Jung, *Tetrahedron* **2001**, 7785–7811.
[55] A. G. Fallis, I. M. Brinza, *Tetrahedron* **1997**, *53*, 17543–17594.
[56] S. Takano, M. Suzuki, A. Kijima, K. Ogasawara, *Tetrahedron Lett.* **1990**, *31*, 2315–2318.
[57] J. Wang, S. Ye, X. Liu, T.-P. Loh, *ACS Sustainable Chem. Eng.* **2020**, *8*, 16283–16295.
[58] T. Alam, A. Rakshit, H. N. Dhara, A. Palai, B. K. Patel, *Org. Lett.* **2022**, *24*, 6619–6624.
[59] D. S. Kulyk, E. Amoah, A. K. Badu-Tawiah, *Anal. Chem.* **2020**, *92*, 15025–15033.
[60] S. Lee, D. S. Kulyk, N. Marano, A. K. Badu-Tawiah, *Anal. Chem.* **2021**, *93*, 2440–2448.
[61] T. A. Kareem, A. A. Kaliani, *Ionics* **2012**, *18*, 315–327.
[62] W. Borsche, *Justus Liebigs Ann. Chem.* **1908**, *359*, 49–80.
[63] A. J. Grooms, A. N. Nordmann, A. K. Badu-Tawiah, *ACS Meas. Sci. Au* **2023**, *3*, 32–44.
[64] A. Venter, P. E. Sojka, R. G. Cooks, *Anal. Chem.* **2006**, *78*, 8549–8555.
[65] a) C. F. Miller, B. J. Burris, A. K. Badu-Tawiah, *J. Am. Soc. Mass Spectrom.* **2020**, *31*, 1499–1508; b) A. Venter, P. E. Sojka, R. G. Cooks, *Anal. Chem.* **2006**, *78*, 8549–8555.
[66] R. R. Sagam, S. K. Nukala, R. Nagavath, N. Sirassu, M. Mohammod, R. Manchal, N. S. Thirukovela, *J. Mol. Struct.* **2022**, *1268*, 133692.
[67] R. Ali, *Tetrahedron* **2023**, *148*, 133692.
[68] S. Kotha, M. Saifuddin, V. R. Aswar, *Org. Biomol. Chem.* **2016**, *14*, 9868–9873.
[69] S. Gore, S. Baskaran, B. König, *Org. Lett.* **2012**, *14*, 4568–4571.
[70] T. Müller, A. Badu-Tawiah, R. G. Cooks, *Angew. Chem. Int. Ed.* **2012**, *51*, 11832–11835.
[71] R. M. Bain, C. J. Pulliam, R. Graham Cooks, *Chem. Sci.* **2015**, *6*, 397–401.

Manuscript received: July 12, 2024
Accepted manuscript online: October 25, 2024
Version of record online: ■■, ■■

Research Article

Microdroplet Chemistry

A. J. Grooms, R. T. Huttner, M. Stockwell, L. Tadese, I. M. Marcelo, A. Kass, A. K. Badu-Tawiah* ——— **e202413122**

Programmable C–N Bond Formation through Radical-Mediated Chemistry in Plasma-Microdroplet Fusion

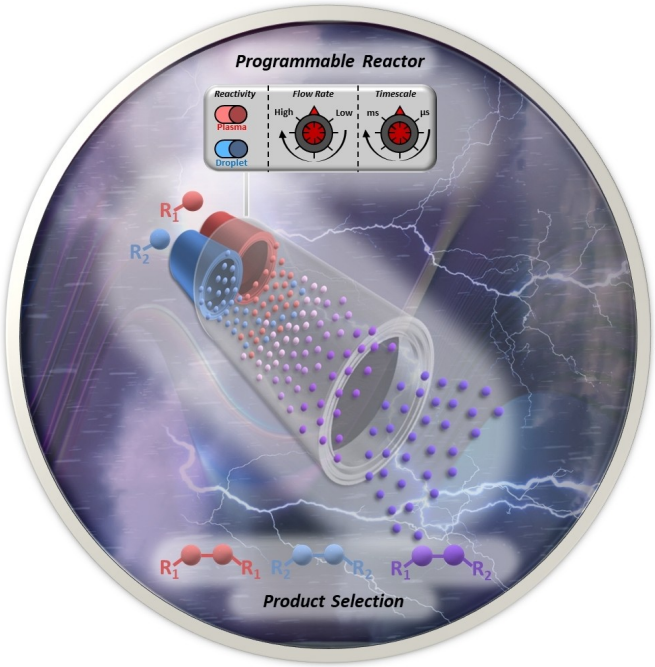

Non-thermal plasma discharge produced in the wake of charged microdroplets is found to facilitate catalyst-free radical mediated hydrazine cross coupling. Plasma-microdroplet fusion occurs online in a programmable reaction platform allowing direct process optimization and product validation via mass spectrometry.